ACS OMEGA

http://pubs.acs.org/journal/acsodf

Article

Graphitic Carbon Nitride Causes Widespread Global Molecular Changes in Epithelial and Fibroblast Cells

Chatterjee Amit, Gajanan Sathe, Abinaya Shunmugam, Prasanna Kumar Athyala, Vivek Ghose, Srujana Chitipothu, Narayanan Janakiraman, Ramaprabhu Sundara,* and Sailaja V. Elchuri*

Cite This: *ACS Omega* 2021, 6, 9368−9380

Read Online

ACCESS | Metrics & More | Article Recommendations | Supporting Information

ABSTRACT: For scaffold and imaging applications, nanomaterials such as graphene and its derivatives have been widely used. Graphitic carbon nitride (g-C_3N_4) is among one such derivative of graphenes, which draws strong consideration due to its physicochemical properties and photocatalytic activity. To use g-C_3N_4 for biological applications, such as molecular imaging or drug delivery, it must interact with the epithelium, cross the epithelial barrier, and then come in contact with the extracellular matrix of the fibroblast cells. Thus, it becomes essential to understand its molecular mechanism of action. Hence, in this study, to understand the molecular reprogramming associated with g-C_3N_4, global gene expression using DNA microarrays and proteomics using tandem mass tag (TMT) labeling and mass spectrometry were performed in epithelial and fibroblast cells, respectively. Our results showed that g-C_3N_4 can cross the epithelial barrier by regulating the adherens junction proteins. Further, using g-C_3N_4−PDMS scaffolds as a mimic of the extracellular matrix for fibroblast cells, the common signaling pathways were identified between the epithelium and fibroblast cells. These pathways include Wnt signaling, integrin signaling, TGF-β signaling, cadherin signaling, oxidative stress response, ubiquitin proteasome pathway, and EGF receptor signaling pathways. These altered signature pathways identified could play a prominent role in g-C_3N_4-mediated cellular interactions in both epithelial and fibroblast cells. Additionally, β catenin, EGFR, and MAP2K2 protein−protein interaction networks could play a prominent role in fibroblast cell proliferation. The findings could further our knowledge on g-C_3N_4-mediated alterations in cellular molecular signatures, enabling the potential use of these materials for biological applications such as molecular imaging and drug delivery.

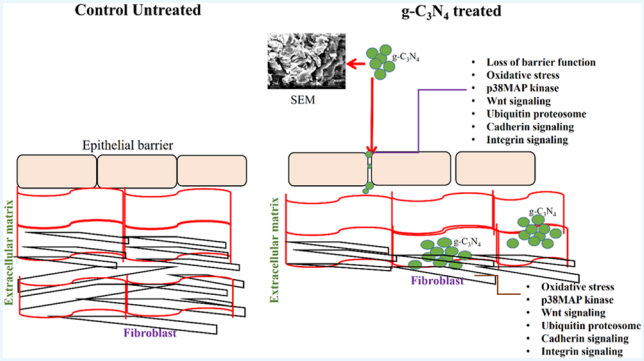

1. INTRODUCTION

Graphene is a two-dimensional sheet of sp^2 hybridized carbons arranged in a honeycomb lattice.[1] Graphene nanoparticles have applications in various fields such as electronics, energy, bioremediation, and nanomedicine.[2] Graphene has a wide array of applications in the field of nanomedicine because of its enormous available surface area, simplicity of functionalization, elevated solubility, exceptional drug-loading capacities, and lipophilic nature.[3] Recently, its communication with the plasma membrane and its uptake mechanism have received considerable attention.[4] The physiochemical properties of graphene play a prominent role in its uptake. The nanomaterials could enter the cells through the process of endocytosis or passive absorbance through the cellular surface.[5]

There are many derivatives of graphene that have been studied widely such as graphene oxide (GO), reduced graphene oxide (rGO), graphane (hydrogenated form of graphene), graphone (semihydrogenated form of graphene), flurographene graphitic carbon nitride, etc. Among the various graphene nanoparticles, GO and rGO have been mostly studied for biological applications, which includes their ability to target cancer stem cells.[6] Additionally, GO is nontoxic to normal fibroblast cells. However, the nanomaterial caused several side effects. At nonlethal concentrations, it induced brain toxicity, mitochondrial damage, and cytoskeleton dysregulation.[7] Treatment of GO and amino-functionalized graphene oxide to immune cells stimulated the polarization of T-cells and initiated immune response.[8]

Graphitic carbon nitride (g-C_3N_4) is widely utilized as a preferred nanomaterial in optoelectronics, energy storage sensors, and photocatalysis.[9] Additionally, it is widely used for pollutant degradation.[10] Bulk synthesis of g-C_3N_4 is obtained by pyrolysis of plentiful nitrogen-containing pre-

Received: November 11, 2020
Accepted: March 23, 2021
Published: April 2, 2021

cursors, such as melamine, thiourea, urea, and cyanamide.[11] Tri-*s*-triazine (C_6N_7) and *S*-triazine (C_3N_3) rings constitute g-C_3N_4 molecules.[12] The carbon and nitrogen atoms in g-C_3N_4 form chemical bonds through sp^2 hybridizations, forming a pie-conjugated delocalized system, and this material is an n-type semiconductor.[13] Recently, its application in photodynamic therapy without utilizing any other molecules as enhancers, for cancer therapy, has been reported. In response to variation in pH, g-C_3N_4 exhibited altered drug release kinetics, enabling its use in delivering drugs efficiently.[14] This nanomaterial has been widely used as a photoelectronic biosensor; for example, Li et al. developed a sensitive method for detecting PKA.[15] g-C_3N_4 nanoparticles have quantum confinement, edge effects, and optical tenability properties, which enable these particles to emit both blue and green lights.[16] Therefore, g-C_3N_4 nanoparticles are widely used for imaging the cells. Further, g-C_3N_4 has also been used as an antiviral substance to treat water-borne diseases.[17] These nanoparticles were made into composites for various applications. The antioxidant property of biological fluids was analyzed by integrating the g-C_3N_4 nanoparticles with polydopamine.[18] AuNPs and g-C_3N_4 composites exhibited excellent peroxidase activity and were used for bacterial wound inactivation.[19] Additionally, g-C_3N_4 nanoparticles possess an advantage as photosensitizers. Its property of a mild band gap of 2.7 eV was used for photodynamic therapy. However, its ability to absorb visible light has practical limitations. Therefore, g-C_3N_4 is combined with high-functioning nanomaterials, such as lanthanide-doped upconversion nanoparticles (UCNPs), for various applications.[20] Additionally, g-C_3N_4 nanoparticles have not been used extensively as cell culture scaffolds because of their structural weaknesses, nonconducting nature, and solubility issues. Therefore, combining these nanoparticles with various polymers has been a new avenue in the field of advanced materials.[21]

The epithelial and fibroblast cells constitute the cellular makeup of organs. Epithelial cells are the first line of defense and are tightly arranged in monolayers. They protect underneath layers, allow diffusion of molecules, and form boundaries.[22] Beneath the epithelium layer, fibroblast cells are located, forming the structural framework of an organ. Fibroblast cells synthesize the extracellular matrix, which acts as a supportive framework for epithelial cells.[23] Epithelial cells containing tight and adherens junctions act as barriers preventing the entry of therapeutic molecules to the stroma where the fibroblast resides. However, nanoparticles, liposomes, and cell-penetrating peptides have the ability to cross the epithelial barrier and reach the stroma.[24−26]

Therefore, it is essential to identify the pathways that are affected by nanoparticles in both epithelial and fibroblast cells.[27] Among various molecules used for delivery or imaging for biological applications, graphene and its derivatives play an important role. Among all of the derivatives of graphene, g-C_3N_4 is the least well-characterized derivative for biological applications. Thus, it becomes important to understand the molecular signaling pathways regulated by g-C_3N_4 and to understand whether the signaling pathways are specific to the material or dependent on the types of cells used for the studies. Therefore, to resolve this issue, we treated g-C_3N_4 to MCF-7 cells that are epithelial in origin and we grew Tenon fibroblast cells on g-C_3N_4−poly(dimethylsiloxane) (PDMS) scaffolds as extracellular mimics for studying molecular changes in both cell types. We studied the signaling pathway induced by g-C_3N_4 in MCF-7 cells using DNA microarrays. Additionally, the global altered protein expression of fibroblast cells grown on g-C_3N_4−PDMS scaffolds was determined by proteomics, using tandem mass tag (TMT) labeling and mass spectrometry. The signaling pathways dysregulated in both cell types were analyzed to identify the specific pathways regulated by g-C_3N_4.

2. MATERIALS AND METHODS

2.1. Synthesis of g-C_3N_4. Graphitic carbon nitrite was prepared as reported earlier by us.[28] Briefly, the material was obtained by heating melamine at 550 °C for 4 h in a tubular furnace in an air atmosphere at a ramp rate of 2.3 °C/min in a ceramic crucible.

2.2. Size Determination of g-C_3N_4 Using Dynamic Light Scattering and Scanning Electron Microscope. The sizes of g-C_3N_4 were measured using Zetasizer Nano ZS (Malvern Instruments, Malvern, U.K.) containing a 4 mW He−Ne laser. The wavelength of measurements was 633 nm. The g-C_3N_4 concentration used for measurements was 1 μg/mL. A 1 cm light path was used, and the intensity of scattered light gathered at the 173° angle enabled surface potential measurement. The hydrodynamic size of g-C_3N_4 was measured in disposable cuvettes.

g-C_3N_4 samples were coated with a 10 nm layer of gold by splutter-coating and imaged using a scanning electron microscope (SEC Co., Ltd., Korea).

2.3. X-ray Diffraction and Fourier Transform Infrared Spectroscopy. X-ray diffraction (XRD) was performed on g-C_3N_4 nanoparticles. The radiation source used was Cu Kα in the 0−50° range. For Fourier transform infrared (FTIR) spectroscopy measurements, g-C_3N_4 dried samples were mixed with KBr for analysis and spectra were recorded using a Bruker Tenzor 27 instrument.

2.4. g-C_3N_4 Uptake in MCF-7. MCF-7 cells were obtained from ATCC, and these cells were maintained in the DMEM medium with 10% FBS. Different concentrations of g-C_3N_4 were treated for 1 and 24 h, and uptakes were studied using a fluorescence microscope (Carl Zeiss, Axio Observer). The uptake of g-C_3N_4 was visualized by TEM measurements after 24 h at a concentration of 50 μg/mL.

2.5. Mitochondrial Localization. MCF-7 cells treated with g-C_3N_4 and TF grown on PDMS−g-C_3N_4 scaffolds along with respective control cells were incubated with a 150 nM mitotracker (M7512, Thermo Fisher). The incubation time was 30 min at 37 °C. The cells were washed with PBS thrice to remove excess stain followed by observations under a fluorescence microscope.

2.6. Microarray Gene Expression Studies in MCF-7 Cells and Data Analysis. Global gene expression analysis was performed using Affymetrix Human Prime view arrays according to the manufacturer's instructions. In total, 2×10^6 MCF-7 cells were seeded and cultured in DMEM supplemented with 10% FBS in triplicates. The cells were washed thrice with 1× PBS and incubated with g-C_3N_4 nanoparticles (50 μg/mL) for 48 h. The cells were washed, trypsinized with 0.01% trypsin−EDTA, and centrifuged at 2000 rpm for 5 min. The pellet was washed twice with 1× PBS; RNA was extracted using an RNeasy mini kit (Qiagen), and RNA was quantified using a nanodrop. A total of 100 ng of RNA was taken to perform the Affymetrix microarray. cDNA and aRNA were synthesized. The aRNA was labeled with biotin, quantified using Bionanospec and fragmented, made a hybridization mixture (130 μL), loaded onto GeneChipPrimeView chip

https://doi.org/10.1021/acsomega.0c05513
ACS Omega 2021, 6, 9368−9380

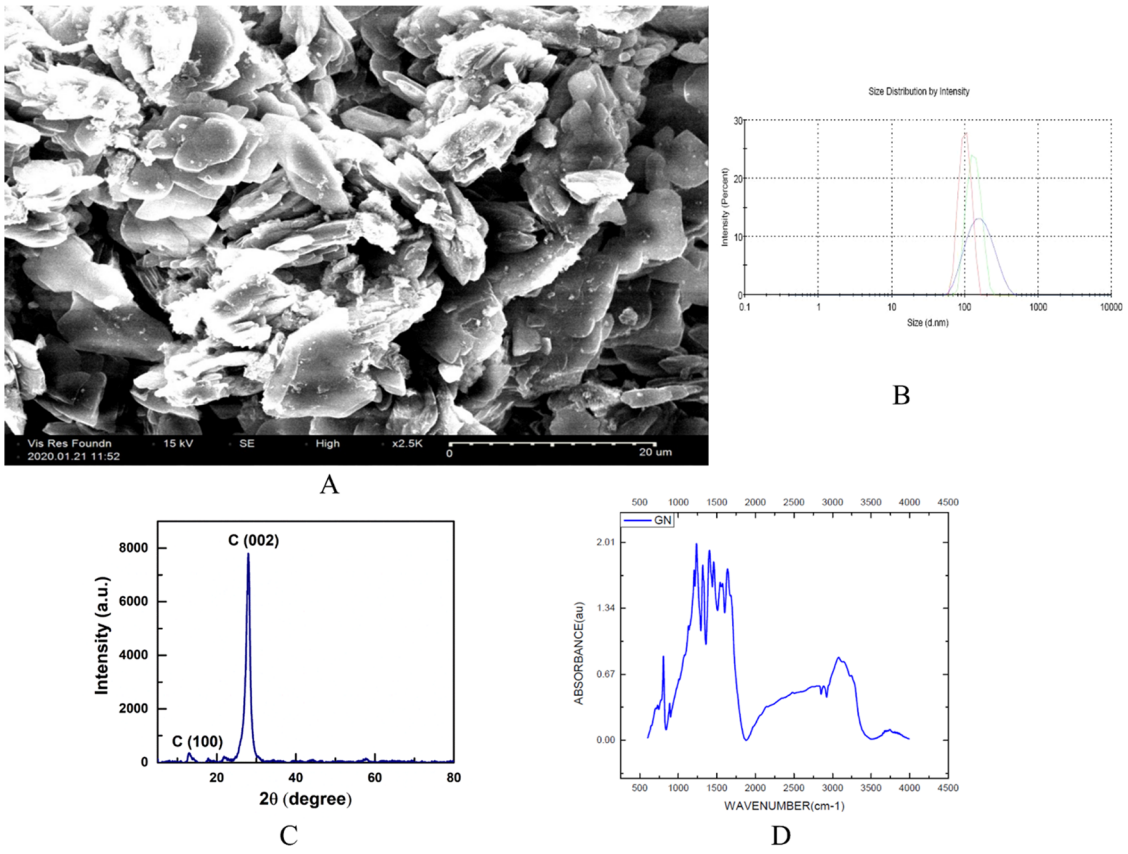

Figure 1. Characterization of g-C_3N_4: (A) scanning electron microscopy analysis; (B) dynamic light scattering analysis; (C) X-ray diffraction; and (D) Fourier transform infrared spectroscopy.

arrays, and hybridized at 45 °C for 16 h using the Affymetrix Gene Chip hybridization oven. The arrays were washed and stained using buffers A, B, and C using Affymetrix fluidic station 450 and scanned for fluorescence signal using the Affymetrix Genechip scanner (3000 G) at 570 nm. The flowchart for the transcriptomics is represented in Figure S1.

2.7. Microarray Data Analysis. The raw files obtained from the scanner were checked again with Affymerix Expression console software (Version 4.0), which generated the .CHP files. The gene expression analysis was performed using Gene Spring Software (Version 13.0) (AgilentTechnologies, Santa Clara, CA). The .CEL files were loaded to gene spring software, and the grouping was done. Quality control was monitored with respect to filtering of the probeset by expression and by error. The normalized raw data was submitted to the NCBI gene expression Omnibus (GSE104939). The statistical analysis was performed individually between the control vs g-C_3N_4 treatments using Gene Spring software (Version 13.0). The data was analyzed using *p*-value 0.02, and multiple testing correlations were done using the Benjamin−Hochberg FDR using default settings. A moderated *t*-test was used for statistical analysis. Gene expression changes greater than 2.0-fold alteration (*p*-value of 0.001) were used for further analysis. Gene ontology (GO) analysis was performed using the FunRich annotation tool and PANTHER. The gene ontology was also performed using the DAVID annotation tool, and KEGG pathways with fold enrichment, *p*-values, and FDR were calculated.

2.8. Western Blotting. The cells were harvested after g-C_3N_4 treatment, and proteins were extracted in RIPA buffer. The proteins were separated by SDS PAGE and blotted onto the nitrocellulose membrane. After blocking primary antibodies β catenin (Abcam-ab22656), E cadherin (CST Cat No. 9961) were treated overnight followed by addition of a secondary antibody for visualization.

2.9. Functionalization of PDMS. The poly(dimethylsiloxane) (PDMS) gel (Sylgard 184 silicone elastomer kit) was prepared in a 1:10 polymer/curing agent ratio. The solution was kept for 24 h at 80 °C for drying and then coated with g-C_3N_4. The dried PDMS scaffold was dipped in 50 μg/mL g-C_3N_4 solution and dried at 60 °C for 1 h. This process was repeated twice more for efficient g-C_3N_4 coating followed by 2 h of drying. The gels were prepared in tissue culture plates for the growth of cells.

2.10. Tenon Fibroblast (TF). Tenon fibroblast cells were isolated from patients undergoing trabeulectomy surgery after the approval by the Institutional Review Board of Vision Research Foundation, Sankara Nethralaya, Chennai, India (Ethics No. 635-2017-P). The tenon fibroblast (TF) cells were grown on TCP-, PDMS-, and PDMS-coated g-C_3N_4. Tenon fibroblast cells were maintained in DMEM F-12 medium having 10% FBS.

2.11. Immunofluorescence. MCF-7 cells were grown for 48 h. g-C_3N_4-treated cells and control cells were used for immunofluorescence studies. Tenon fibroblast cells were grown on g-C_3N_4−PDMS scaffolds for 72 h. The cells grown on tissue culture plates served as controls for these cells. They were fixed in 4% paraformaldehyde, permeabilized with 0.5% triton-100 followed by PBS washing. The cells were blocked with 1% BSA for 1 h followed by overnight incubation with the

https://doi.org/10.1021/acsomega.0c05513
ACS Omega 2021, 6, 9368−9380

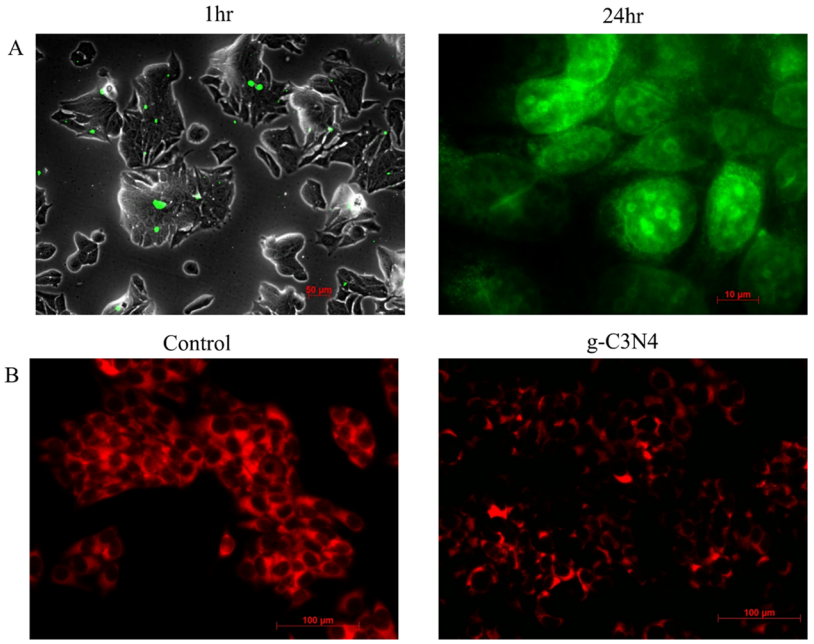

Figure 2. g-C_3N_4 uptake and its effect: (A) uptake of g-C_3N_4 in MCF-7 cells in 1 and 24 h; (B) mitotracker staining of the control and g-C_3N_4 in MCF-7 cells.

primary antibody pCDC25C (Thermo Fisher Cat No. PA5-38358) and Vimentin (CST Cat No. 5741) for MCF-7 and TF cells, respectively. The Cy3.5-labeled secondary antibody was used for detection by fluorescence microscopy. The cell nuclei were counterstained with Hoechst fluorescent stain (Thermo Fisher Cat No. 33342).

2.12. TMT Labeling and Proteomics of TF. The flowchart for proteomics is represented in Figure S1. The cells grown on the graphene and control tissue culture plates were lysed in 4% SDS. The control and graphene protein samples were reduced and alkylated in equal amounts. Then, the proteins were precipitated with ice-cold acetone. Proteins were digested in lys-C (1:100) for a period of 4 h and treated with trypsin digestion at a 1:20 ratio for a 12−16 h period at 37 °C temperature. The Sep-Pak C_{18} column material was used for peptide purification. These peptides were labeled using TMT tags according to the manufacturer's instructions (Catalog No. 90110, Thermo Fisher Scientific). TMT tags 126, 127, and 128 were used to label control samples, and graphene samples were labeled with TMT tags 129, 130, and 131. Then, the samples were pooled and analyzed on the mass spectrometer (Orbitrap Fusion Tribrid mass spectrometer, Thermo Scientific, Bremen, Germany) interfaced with a liquid chromatography system (Easy-nLC 1200 nanoflow, Thermo Scientific, Bremen, Germany). Peptides were separated on 75 μm × 50 cm (RSLC C18) analytical columns. The flow rate of the elluted peptides was 300 nL/min. Then, 8−35% solvent B (0.1% formic acid in 95% acetonitrile) gradient was used for 103 min to separate proteins. The data-dependent acquisition mode was used during mass spectrometer running. Following are the parameters used for the mass spectrometer analysis. For MS_1 analysis, the AGC target is 4×10^5, resolution 120 K, 350−1600 scan range. For MS_2 analysis resolution 50 K, the AGC target is 1×10^5, ion filling time is 100 ms, the isolation window is 1.6, and the collision energy HCD is 34. Dynamic exclusion was set for 30 s with a 10 ppm mass window. The acquired mass spectrometry data were searched against the Human RefSeq protein database with common contaminants using the SEQUEST search algorithm and using the Proteome Discoverer platform (version 2.1, Thermo Scientific). The search parameters were two missed cleavages, carbamidomethylation at cysteine, and addition of 229.163 mass for the TMT label. The modifications at the N-terminus of the peptide and lysine were set as fixed modifications. The oxidation of methionine was considered as a variable modification. The monoisotopic peptide mass tolerance was set to 10 ppm and the MS/MS tolerance was set to 0.05 Da for the data analysis. The false discovery rate at the PSM and protein levels was 1%. Statistical analysis was performed using the Perseus software package. The mass spectrometry data have been deposited in the PRIDE database with accession number PXD023061.

2.13. Bioinformatic Analysis. The gene ontology for proteomics and microarray was performed using FunRich and PANTHER.[29,30] Gene IDs of the identified list of genes and proteins were recovered and were applied using the online databases to identify the pathways and for comparison analysis. Protein−protein interactions were studied in the STRING online database at the highest confidence level of 0.9. The network was clustered employing *K*-means clustering in the STRING database to identify prominent interacting networks.

3. RESULTS AND DISCUSSIONS

3.1. g-C_3N_4 Characterization. The SEM images from g-C_3N_4 exhibited an irregular shape and stacking (Figure 1A). The g-C_3N_4 surface morphology is similar to that of our previously published material.[28] Further, the hydrodynamic size of the synthesized g-C_3N_4 material was found to be 100 nm size (Figure 1B). The phase characterization of g-C_3N_4 was analyzed using XRD (Figure 1C). Peaks were observed at 2θ = 13.1 and 27.3° planes. The 13.1° peak represents the packing motif of tris-*s* triazane, whereas 27.3° corresponds to the reflection characteristics of interlayer stacking of the conjugated aromatic system.[31] Peaks were observed between

https://doi.org/10.1021/acsomega.0c05513
ACS Omega 2021, 6, 9368−9380

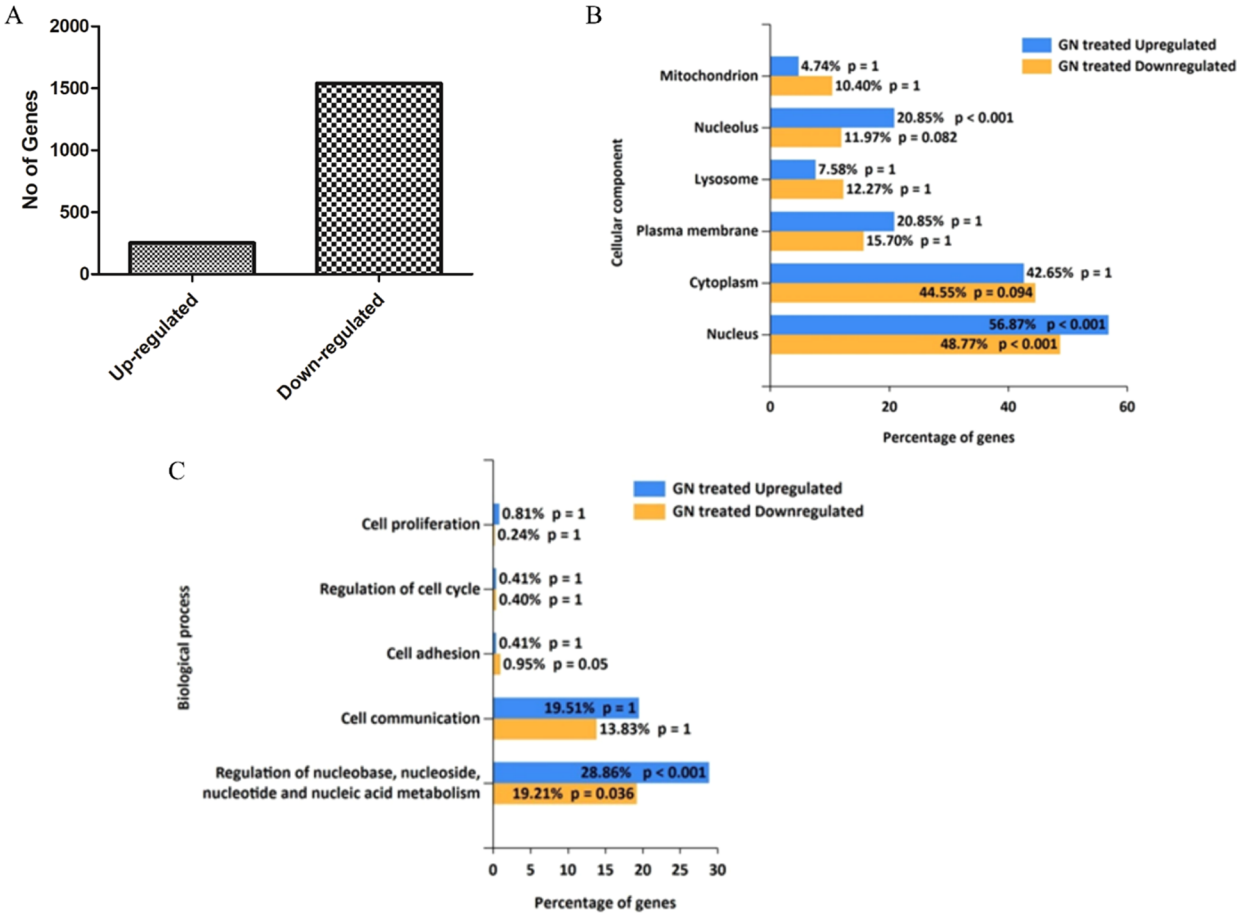

Figure 3. g-C_3N_4 uptake causes alteration in cell signaling pathways. (A) Upregulated and downregulated genes by DNA microarray analysis. (B) Functional enrichment analysis of the cellular component by upregulated and downregulated genes. (C) Functional enrichment analysis of biological processes by upregulated and downregulated genes. "p" is used by the online tool to perform the statistical analysis between the pathways. *p*-Values <0.05, <0.01, and <0.001 are significantly altered pathways.

1200 and 1650 cm^{-1} by FTIR spectroscopy. These were attributed to stretching of aromatic C−N heterocycles present in g-C_3N_4 (Figure 1D). Additionally, 1226 and 1315 cm^{-1} peaks were also observed, which could come from vibrations from secondary and tertiary amine fragments, respectively.[32] The Raman spectra from g-C_3N_4 did not exhibit any considerable peaks by our earlier study due to fluorescence from the particles.[28,33] The carbon and nitrogen atomic percentages in the material were 45 and 55%, respectively.[34] Our earlier thermogravimetric analysis performed on g-C_3N_4 revealed stability up to 600 °C,[28,34] indicating these to be ideal for biological experiments. Therefore, in this study, we analyzed the molecular changes associated with the uptake of g-C_3N_4.

3.2. Uptake of g-C_3N_4 by Cells. After characterization of g-C_3N_4, we studied its uptake in two different cell lines MCF-7 and NCC-RbC-51 at two time points of 1 and 24 h for understanding the rapid and sustained uptake. g-C_3N_4 uptake was minimal within 1 h of exposure to the cells (Figure 2A), and the uptake increased after 24 h (Figure 2A). Our results agree with earlier studies with g-C_3N_4−Au composites where the uptake was performed for a duration of 24 h.[35] MCF-7 cells were used as an example for epithelial cells in further studies. g-C_3N_4 was observed to have both cytosol and nuclear localization, indicating possible material molecular interactions inside the cellular organelles by TEM measurements (Figure S2). The nuclear localization of the material strongly indicates its role in regulating the gene expression changes in the cells. As graphene and its derivatives have been reported to cause a reduction in the mitochondrial membrane potential,[36] we analyzed the effect of g-C_3N_4 on mitochondria by studying the accumulation of the mitotracker red dye in MCF-7 cells, as the dye accumulation is known to be affected by the mitochondrial potential. Figure 2B indicates that in g-C_3N_4-treated MCF-7 cells there is a lowered accumulation of the mitotracker red dye. Previous studies reported ROS-mediated stress, mitochondrial functional loss,[37] and damage to macromolecules such as DNA in cells treated with graphene and its derivatives.[38,39] Thus, to understand the signaling pathways regulated by g-C_3N_4 in MCF-7 cells, we performed DNA microarray analysis to identify the global transcriptomic signature of g-C_3N_4 treatment in epithelial cells.

3.3. Global Gene Expression Analysis Identified Extensive Changes after g-C_3N_4 Uptake in MCF-7 Cells. The global gene expression analysis was undertaken using DNA microarrays at 50 μg/mL g-C_3N_4 treatment after 24 h as the cells showed the uptake only after 24 h, and at this concentration, the mitochondrial potential was altered. Alterations in 1789 gene expressions with greater than 2-fold dysregulation were found in the g-C_3N_4-treated cells compared to the control MCF-7 cells (Table S1). There were 252 genes that exhibited upregulation, whereas 1537 genes exhibited

https://doi.org/10.1021/acsomega.0c05513
ACS Omega 2021, 6, 9368−9380

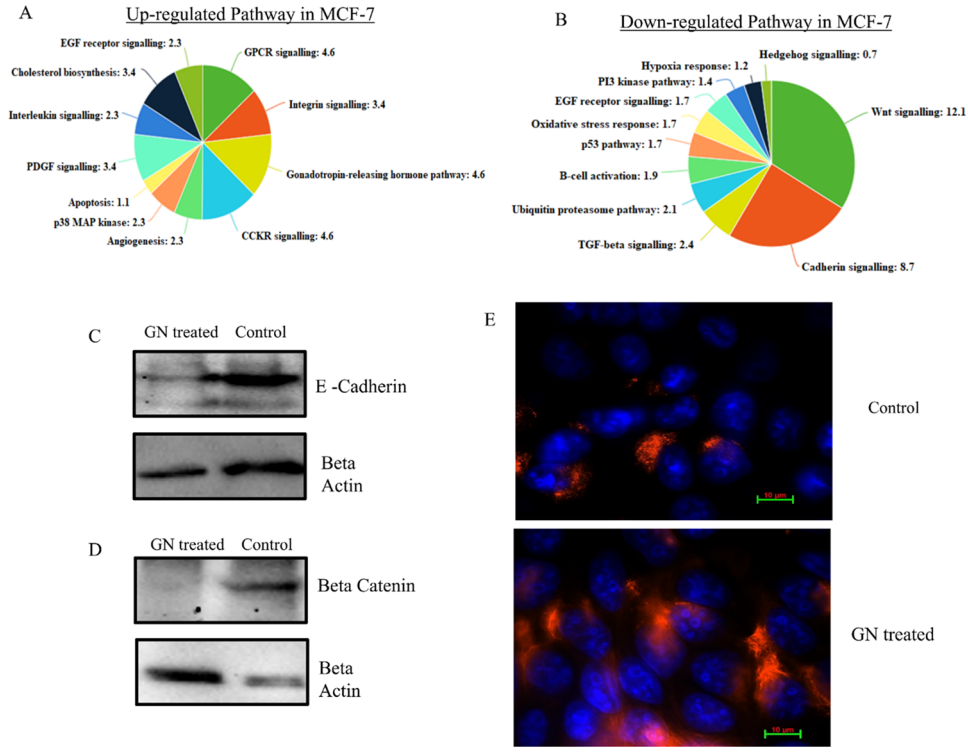

Figure 4. Pathway analysis using g-C_3N_4 in MCF-7 cells. (A, B) PANTHER pathway analysis of upregulated and downregulated genes, respectively. (C, D) Immunoblotting of E cadherin and β catenin from g-C_3N_4-treated and control MCF-7 cells. (E) Phospho-CDC25C protein expression in g-C_3N_4-treated and control MCF-7 cells using fluorescence microscopy.

downregulation (Figure 3A). The heat map for the gene expression analysis and hierarchical clustering was done using Genespring software analysis, indicating that control samples (N = 3) clustered together and g-C_3N_4-treated MCF-7 cells (N = 3) clustered as a group (Figure S3). The gene ontology performed using DAVID functional annotation tools consisted of interstrand cross-link repair, response to ionizing radiation, mRNA export, protein N-linked glycosylation via asparagine, negative regulation of the KJK cascade, and apoptotic signaling pathway mediated through P53 as affected biological processes (Table S2). Upregulated and downregulated genes were segregated and were studied using PANTHER and FunRich 3.0 tools. Both the upregulated and downregulated genes affected the nucleus of the cells, whereas the nucleolus was significantly altered by upregulated genes (Figure 3B). Similar to g-C_3N_4, another graphene derivative graphene oxide has been reported to cause nuclear perturbations and altered its shape in skin keratinocytes.[40] Several (10.40%) downregulated genes after the g-C_3N_4 treatment affected the mitochondria. The loss of mitochondrial staining is known to be due to both structural and functional loss of mitochondria.[41] Similar to our results, pristine graphene treatment in U87 glioma cells caused dysfunctional mitochondria.[42] Furthermore, analysis of altered biological processes revealed cell adhesion and nucleotide metabolism after g-C_3N_4 treatment (Figure 3C). Recently, three-dimensional graphene foam has been reported to regulate the nucleotide metabolism of neural stem cells.[43] The pathways identified using PANTHER analysis revealed changes in the cellular signaling and angiogenesis pathways. Furthermore, upregulated genes were involved in GPCR, integrin, EGF receptor, and p38 MAP kinase signaling pathways (Figure 4A), whereas downregulated genes were involved in cadherin signaling, Wnt signaling, PI3 kinase pathway, oxidative stress response, TGF-β signaling, and p53 pathway (Figure 4B). The alteration of the MAPK pathway could result in dysregulated cellular proliferation (Figure S4). On further analysis, the key downregulated genes were dual-specificity MAP kinase phosphatases 28 (DUSP28), STYXL1, MAP2K4, MYC, and STYX. DUSP28 plays a key role in regulating dephosphorylation and inactivation of MAP kinase isoforms while controlling oxidative phosphorylation and mitochondrial dysfunction.[44] These changes together can alter cell adhesion and cell proliferation. The pathway analysis indicates cadherin and Wnt signaling that regulate these processes to be downregulated.[45] Furthermore, downregulation of the TGF-β signaling pathway was observed in g-C_3N_4-treated MCF-7 cells consisting of SMAD 1, 2, 6 genes (Table S3). The transforming growth factor β (TGF-β) expression increases in all fibrotic diseases, and it also increases ROS production and suppresses antioxidant enzymes.[46] However, recently, reciprocal regulation of SMAD-dependent TGF-β signaling has also been reported.[46] We could envisage such a regulation by SMAD genes in regulating TGF-β signaling in g-C_3N_4-treated cells. Further, KEGG pathway analysis has revealed dysregulation of viral carcinogenesis, mRNA surveillance pathway, cell cycle, transcriptional misregulation of cancer, RNA transport, and ribosome biogenesis as interesting, dysregulated pathways, with high fold enrichment and low FDR (Table S4), indicating that pathways related to transcription, transport of mRNA, and translation of proteins could be effected, leading to ribosome functional dysregulation after g-C_3N_4 uptake.

3.4. Proteins Related to Wnt Signaling and Cell Cycle Are Dysregulated in Epithelial Cells. The alteration in cell adhesion and proliferation enabled us to study the key molecules associated with this pathway. Microarray data

https://doi.org/10.1021/acsomega.0c05513
ACS Omega 2021, 6, 9368−9380

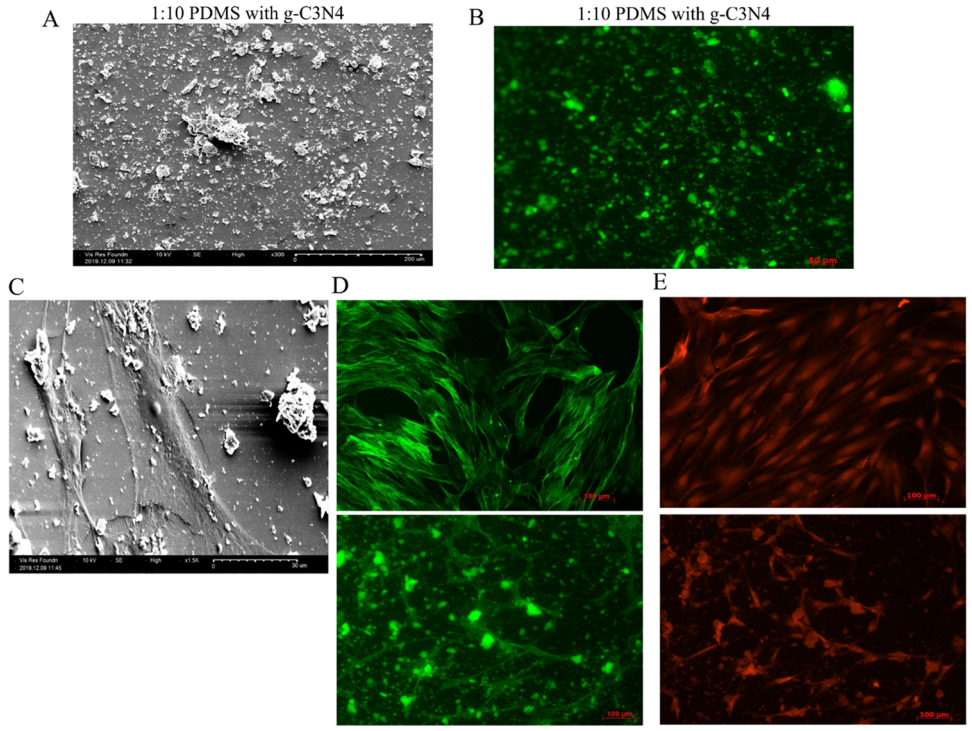

Figure 5. Efficient growth of fibroblast cells on g-C_3N_4−PDMS composite scaffolds. (A) SEM of g-C_3N_4-functionalized PDMS. (B) Fluorescence microscopy of g-C_3N_4-functionalized PDMS. (C) SEM of TF cells grown on g-C_3N_4-functionalized PDMS. (D) Phalloidin staining of cells grown on TCP and g-C_3N_4-functionalized PDMS scaffolds. (E) Mitotracker staining of cells on TCP, PDMS, and g-C_3N_4-functionalized PDMS scaffolds.

showed that the Wnt signaling pathway is downregulated. Wnt signaling plays a vital role in cell adhesion and transcriptional control. Additionally, cadherin signaling was altered. Therefore, we validated β catenin and E cadherin protein expressions after g-C_3N_4 treatment as representative molecules for these signaling pathways. We observed that after 24 h there was a reduction in their protein expressions (Figure 4C,D). The cell-cycle progression was altered in addition to dysregulation in cell adhesion by transcriptomic analysis. Therefore, we analyzed the CDC25c ser215 phosphorylation status in g-C_3N_4-treated cells to understand key phosphorylated proteins that regulate cell-cycle progression. The CDC25 class of proteins are phosphatases that play a major role in mitosis progression, and their activities are regulated by phosphorylation and dephosphorylation at specific amino acid moities.[47] These proteins are in the inactive form when they are hypophosphorylated and become active when they are hyperphosphorylated.[48] The g-C_3N_4 treatment resulted in upregulation of phospho CDC25C (Figure 4E). This indicates a crosstalk between cell-cycle progression and cell adhesion mediated by g-C_3N_4.

3.5. Growth of Fibroblast Cells on g-C_3N_4-Functionalized PDMS Scaffolds. Treatment of g-C_3N_4 in epithelial cells caused a decrease in TGF-β signaling, an increase in oxidative stress response, and altered the cellular adhesion. Pristine and oxidized graphene are nontoxic to fibroblast cells and have been reported to support the proliferation of skin fibroblasts and regeneration.[49] Our results indicated that g-C_3N_4 can cross the epithelium barrier; therefore, we functionalized g-C_3N_4 on the poly(dimethylsiloxane) (PDMS) surface to grow fibroblasts. In the physiological condition, once the epithelial barrier is broken, the material interacts with the extracellular matrix of the fibroblasts. Therefore, g-C_3N_4-functionalized PDMS was used for growth of fibroblast cells. PDMS has been widely used as a scaffold to culture fibroblasts, melanocytes, and different other cell lines.[50] Previously, PDMS was made as a composite with GO sheets using a hydrosilylation reaction and a hydrolysis condensation reaction.[51] These nanocomposites were also prepared using simple curing and vacuum.[52] The latter methodology was presently used to prepare the g-C_3N_4−PDMS composites. The functionalization of g-C_3N_4 in PDMS scaffolds was observed using SEM (Figure 5A). The functionalization by nanoparticles made the PDMS surface rough, and the scaffold exhibited fluorescence (Figure 5B). Further, tenon fibroblast (TF) cells, collected from patients undergoing trabeculectomy, were seeded on g-C_3N_4-functionalized PDMS for 3 days. The TF cells attached and grew well on these scaffolds. The cells could be visualized by SEM micrographs (Figure 5C). Actin staining was performed to show that the cells were attached on g-C_3N_4−PDMS composites (Figure 5D). However, due to the fluorescence property of g-C_3N_4, the g-C_3N_4−PDMS composites showed background fluorescence. The PDMS polymer is known to be hydrophobic, and for attaching cells on its surface, either plasma treatment or extracellular matrix proteins such as collagen or fibronectin coatings were needed.[53] However, our results showed that on the g-C_3N_4-functionalized PDMS matrix, the cell attachment was higher without the ECM coating material. Similarly, the mitochondrial staining pattern differed from tissue-culture-grown cells (Figure 5E). The mitochondrial staining indicates robust mitochondrial function in both TCP and scaffold-grown cells. An altered morphology of TF cells was observed in 1:10 PDMS-grown cells. However, g-C_3N_4 functionalization altered the matrix stiffness of PDMS, enabling the recovered morphology of the TF. Therefore, g-C_3N_4 functionalization could be better for growing fibroblast cells compared to PDMS alone. This scaffold was used for further studies. The altered morphology of the cells cultured

https://doi.org/10.1021/acsomega.0c05513
ACS Omega 2021, 6, 9368−9380

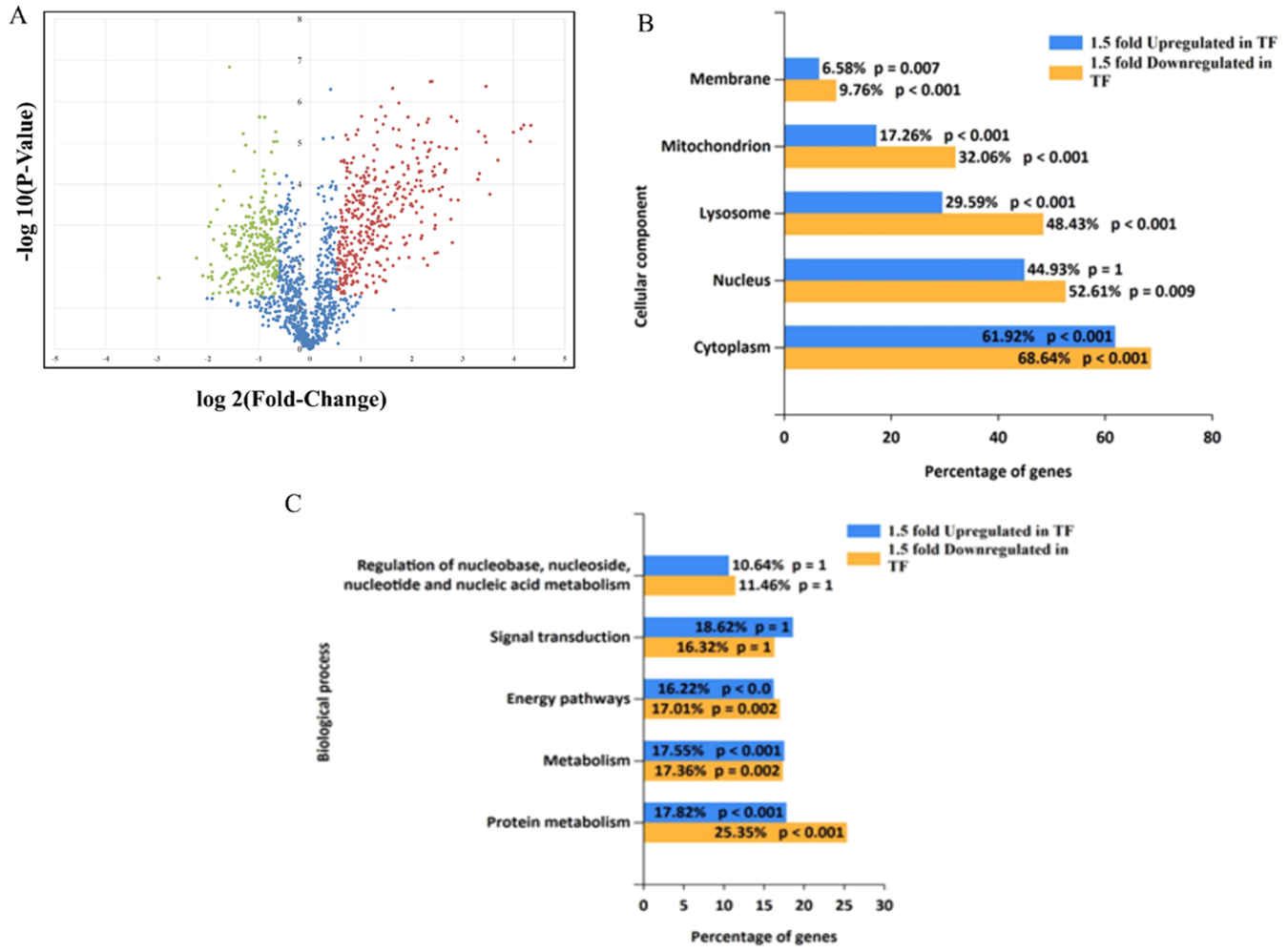

Figure 6. Global proteomic changes in fibroblast cells grown on g-C_3N_4−PDMS scaffolds compared to control cells identified widespread changes in cellular and biological processes. (A) Volcano plot to show the differentially regulated proteins in TF grown on g-C_3N_4−PDMS. Protein expressions are as follows: yellow, downregulated; blue, no change; and red, upregulated. (B) Cellular components of upregulated and downregulated proteins in TF. (C) Biological processes of upregulated and downregulated proteins in TF. "p" is used by the online tool to perform the statistical analysis between the pathways. *p*-Values <0.05, <0.01, and <0.001 are significantly altered pathways.

on g-C_3N_4-functionalized PDMS appeared to be more differentiated.[54] Therefore, to further analyze the global protein expression changes, we performed proteomics using tandem mass tag (TMT) labeling and mass spectrometry.

3.6. g-C_3N_4 in the Extracellular Matrix Can Cause Proteomic Dysregulation in Fibroblasts. Changes in cell attachment in response to varied matrix stiffnesses led us to investigate global proteomic changes associated with fibroblast cells grown on g-C_3N_4-functionalized PDMS using fibroblast cells cultured on tissue culture plates as a control. Proteomic analysis identified 1713 proteins in fibroblast cells grown on PDMS−g-C_3N_4 compared to control cells (Table S5). However, 676 proteins exhibited ≥1.5-fold alterations in protein expression. The expressions of 382 proteins were upregulated and 294 proteins were downregulated compared to the protein expressions in the control fibroblast cells grown on tissue culture plates. The protein expressions were represented in a Volcano plot (Figure 6A). The protein expressions varied significantly in g-C_3N_4−PDMS scaffold-grown fibroblasts compared to the control cells grown on the TCP plate. The dysregulated genes were analyzed using PANTHER bioinformatic analyses and the functional enrichment tool (FunRich). In total, 676 proteins exhibiting ≥1.5-fold alterations were segregated into upregulated (382) and downregulated (294) protein expressions compared to the protein expression in the control TCP-plate-grown cells. The gene ontology analysis identified that both upregulated and downregulated proteins affected mitochondria, cytoplasm, and the nuclear functions, similar to MCF-7 cells (Figure 6B). However, the proteins localized to the plasma membrane were significantly downregulated in fibroblast cells. The altered plasma membrane protein expression identified in the TF could be due to the change in the matrix stiffness mediated by g-C_3N_4 present exterior to the cells. On further annotating the biological process, both upregulated and downregulated proteins altered the protein metabolism and energy pathways (Figure 6C).

The KEGG pathway analysis with greater fold enrichment and low FDR identified dysregulation in the ribosome, protein processing in the endoplasmic reticulum, spliceosome, carbon metabolism, endocytosis, cytoskeletal rearrangement, and adherens junction pathways (Table S6). Further, upregulated and downregulated proteins were segregated, and pathway analyses were performed using the PANTHER online tool. Analysis showed altered integrin signaling, gonadotropin-releasing pathway, ubiquitin proteasome pathway, Wnt signal-

https://doi.org/10.1021/acsomega.0c05513
ACS Omega 2021, 6, 9368−9380

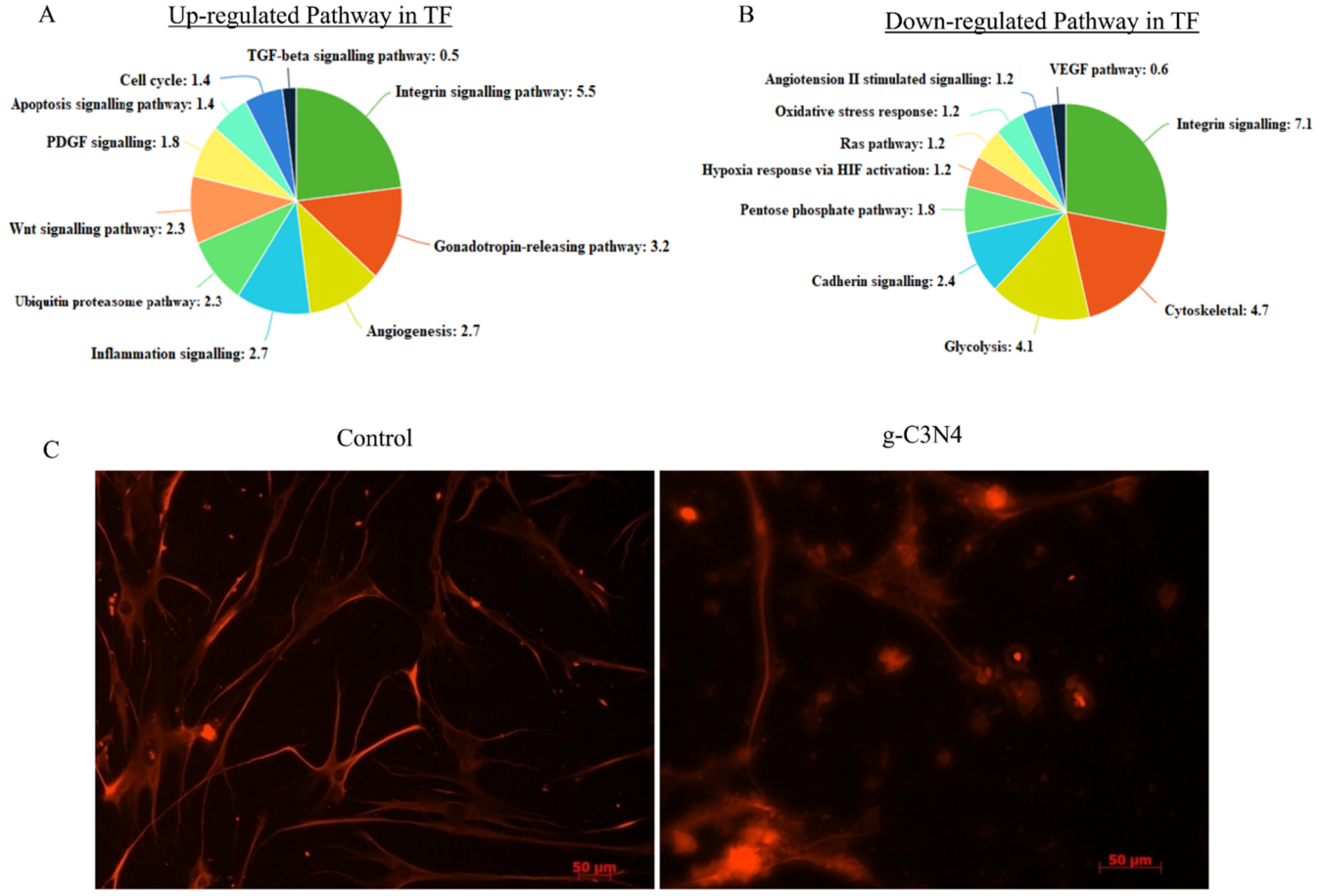

Figure 7. Pathways dysregulated in scaffold-grown fibroblasts compared to the control. (A, B) PANTHER pathway analysis by upregulated and downregulated proteins of g-C_3N_4-functionalized PDMS. (C) Immunofluorescence validation of Vimentin identified by mass spectrometry.

ing, apoptosis, cell cycle, and TGF-β signaling (Figure 7A). Wnt signaling, which was found downregulated in epithelial cells by the microarray, was found to be upregulated in TF. Next, we analyzed the proteins identified in this pathway. Our data showed β catenin, follistatin-related protein 1, serine/threonine-protein phosphatase 2B, and calcineurin subunit B to be dysregulated. This signaling plays an important role in fibroblast differentiation to myofibroblasts. Tumor cells when cocultured with fibroblasts are known to induce a myofibroblast phenotype and altered TGF-β signaling in fibroblast cells.[55] Interestingly, MAPK3, identified in the TGF-β signaling pathway (Tables S3 and S5), could play a role in increased cellular proliferation. The downregulated proteins showed an altered integrin pathway, cytoskeletal reorganization, cadherin signaling, oxidative stress response, hypoxia, and metabolic pathways such as glycolysis and pentose phosphate pathways (Figure 7B). On further analysis of the proteins associated with oxidative stress, a thioredoxin-1 like protein (TXNL1) was identified. This protein is a reductase that plays a vital role in the degradation of proteins, reduces oxidative phosphatase, and can stimulate oxidative stress resistance.[56] Additionally, thioredoxin (TXN) antioxidant proteins involved in redox metabolism are downregulated (Table S5). The principal proteins of oxidative stress response TXNL1 and TXN were downregulated as elevated ROS may not be present and need for antioxidants could be diminished.[57] Alternatively, antioxidant glutathione levels could be elevated by increased glutathione synthetase and glutathione reductase levels (Table S5). Elevated glutathione could enable fibroblast cell growth. Its depletion in RPE cells was found to increase ferroptosis, autophagy, and cell death.[58] HIF signaling is known to be a pivotal link among energy metabolism, angiogenesis, cell proliferation, and viability.[59] Interestingly, downregulation of the HIF pathway could account for the lowered glycolysis observed in fibroblast cells, enabling sustained growth of cells. Stem cells cultured on reduced O_2 enabled downregulation of HIF-1a, leading to a metabolic switch from glcolysis; moreover, decrease in ROS levels enabled reduced DNA damage, resulting in long-term growth of the cells.[60] Earlier, the graphene family nanomaterial GO was proposed to be an efficient ROS scavenger enabling cardiac tissue growth and repair.[61] Taken together, our global proteomic analysis indicates that g-C_3N_4 in the scaffolds could efficiently scavenge ROS and enable fibroblast cell growth. Interestingly, in both the epithelium and TF cells, when g-C_3N_4 were treated or formed a scaffold for cell growth, it induced downregulation of genes and proteins associated with cadherin signaling, indicating alterations in ECM regulation. Further, the altered morphology and the proteomics data were validated using Vimentin staining as this protein expression was reported to be a differentiation marker.[62] The TF cell culture on g-C_3N_4-functionalized PDMS showed a positive staining for Vimentin (Figure 7C). However, the pattern of staining is diffused, indicating the possibility of differentiation of fibroblast cells.

3.7. Protein−Protein Interaction Networks. Next, we analyzed protein−protein interaction networks to understand

https://doi.org/10.1021/acsomega.0c05513
ACS Omega 2021, 6, 9368−9380

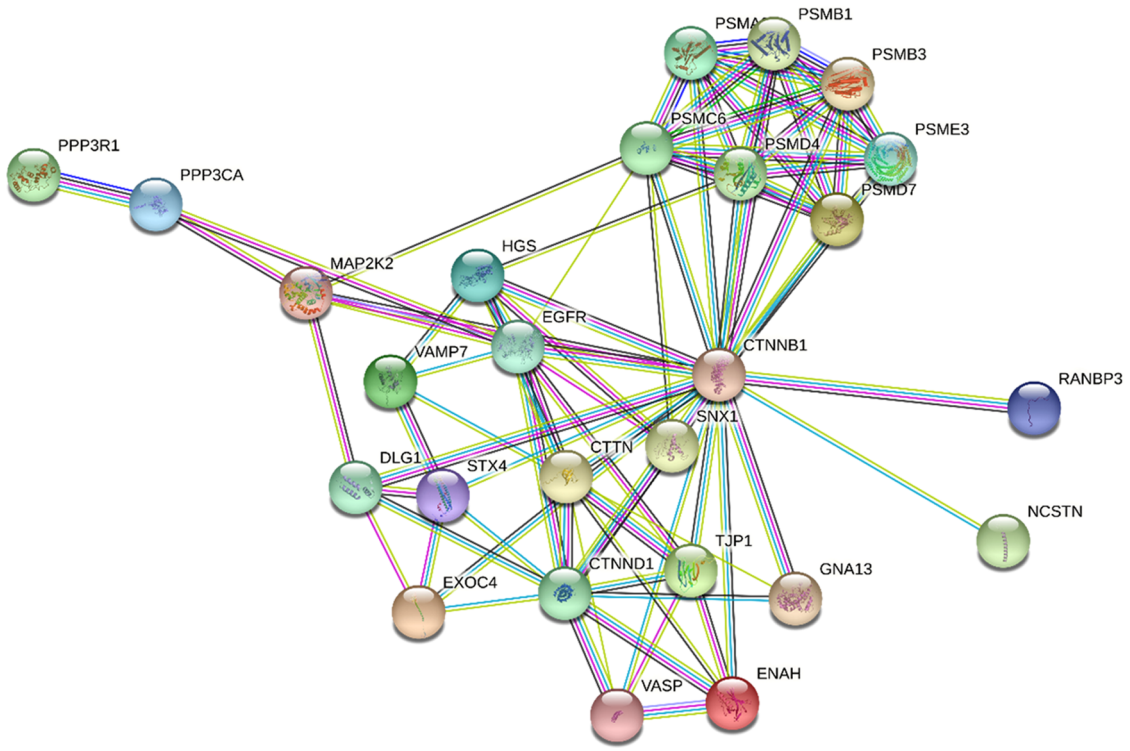

Figure 8. β Catenin protein−protein interaction cluster is upregulated in fibroblast cells grown on g-C_3N_4-functionalized PDMS.

the key networks associated with g-C_3N_4 in fibroblasts using STRING database analysis. The upregulated protein network contained 378 nodes and 678 edges (Figure S5). Using the *K*-mean clustering algorithm, prominent 10 network clusters were identified. The prominent interaction clusters comprised mRNA processing, RNA processing, elongation factors, collagen, and MAPK3. Interestingly, β catenin and its interacting partners comprising MAP2K2 and EGFR are also identified (Figure 8). This interaction could account for fibroblast proliferation on PDMS−g-C_3N_4 scaffolds. The downregulated protein network had 292 nodes and 1472 edges. The clustering interactions included protein interactions from splisosome, ribosomes, metabolism including glycolysis and pentose phosphate pathway, and vesicular trafficking (Figure S6). Interestingly, oxidative stress response genes such as SOD1, SOD2, GPX8, and PRDX family genes (PRDX1, PRDX2, PRDX3, PRDX5) clustered together. The switch of metabolic interactions into lowered ROS-responsive genes and lowered glycolysis is adaptive mechanisms by fibroblast cells during efficient growth, proliferation, and differentiation in fibroblasts into myofibroblasts. The regulatory role of g-C_3N_4 in inducing the differentiation of fibroblasts needs further investigation.

3.8. g-C_3N_4 Signature Pathways. A comparison of pathways dysregulated using the Panther pathway analysis tool between global transcriptomic and proteomic changes associated with the g-C_3N_4 nanomaterial identified 47 pathways common between the two analyses (Figure S7, Table S7). The predominant alterations were observed in several key pathways related to cellular proliferation, apoptosis, and cell adhesion. These include Wnt signaling, integrin, TGF-β, cadherin, oxidative stress response, and ubiquitin proteosome pathway alterations in both epithelial and fibroblast cells (Table S7). The pathways are either upregulated or downregulated based upon the presence of nanomaterials inside or outside the cell in the scaffolds.

4. CONCLUSIONS

Poly(dimethylsiloxane) (PDMS) is a silicone elastomer and has been used as a substrate for various cell culture studies. The elastic modulus of PDMS is known to induce changes in the tenon fibroblasts. PDMS as a control would have been excellent, but one major difficulty was that cells were not attached to PDMS due to its hydrophobic nature and coating with ECM proteins would have induced gene expression changes, as reported earlier. Primary human tenon fibroblasts (TFs) have been reported to respond differentially to different extracellular matrix protein gels, which in turn causes their differentiation. Interestingly, g-C_3N_4−PDMS did not require functionalization with extracellular matrix proteins, and cells showed good adhesion as shown by Phallodin staining.

Our results indicate that the synthesized pure g-C_3N_4 can cross the barrier formed by the epithelial cells. Its treatment in epithelial cells induced elevated ROS, alterations in cellular adhesion, proliferation, and loss of barrier function in the epithelial cells. Beneath the epithelium is the fibroblast, which is known to synthesize the components of the extracellular matrix. The changes in the elasticity and composition of the extracellular matrix are known to initiate fibrosis. Therefore, g-C_3N_4 is used in the matrix scaffolds to identify its role in initiating molecular proteomic dysregulation.

The nanoparticles' presence in the ECM can cause changes in the molecular programming of fibroblast layers beneath the epithelial cells. We deciphered the specific pathways altered by g-C_3N_4 using two different cell lines, epithelial (MCF-7) and fibroblast (TF) cells. We used two different ways of treatment of the same concentration of g-C_3N_4. Directly treating MCF-7 and functionalizing g-C_3N_4 on PDMS to use it as a matrix. We observed common signaling pathways such as Wnt signaling,

https://doi.org/10.1021/acsomega.0c05513
ACS Omega 2021, 6, 9368−9380

integrin signaling, TGF-β signaling, cadherin signaling, oxidative stress response, ubiquitin proteasome pathway, and EGF receptor signaling pathways to be affected in both cell lines. Our results should enable the wider application of g-C_3N_4 after our molecular pathway analysis.

■ ASSOCIATED CONTENT

Supporting Information

The Supporting Information is available free of charge at https://pubs.acs.org/doi/10.1021/acsomega.0c05513.

Global transcriptomics in epithelial cells (MCF-7) and proteomics in fibroblast cells using DNA microarrays and TMT labeling followed by mass spectrometry in triplicates; uptake of g-C_3N_4 nanoparticles in MCF-7 using TEM measurements after 24 h at a concentration of 50 μg/mL; histogram of global gene expression changes performed using Genespring software indicating widespread changes after g-C_3N_4 treatment in MCF-7 cells; visualization of MAP kinase pathway alteration in MCF-7 cells after g-C_3N_4 treatment (KEGG pathway representation); clustered protein−protein interaction network of upregulated proteins in the fibroblasts grown on PDMS−g-C_3N_4 scaffolds; clustered protein−protein interaction network of downregulated genes in g-C_3N_4 fibroblasts grown on PDMS−g-C_3N_4 scaffolds; pathway comparison between global changes in transcriptomics and proteomics performed by DNA microarray analysis and TMT labeling followed by mass spectrometry (PDF)

Global gene expression changes altered in MCF-7 cells treated with g-C_3N_4-fold changes of control vs g-C_3N_4 treatment by Genespring analysis; gene ontology—biological processes dysregulated in MCF-7 cells treated with g-C_3N_4 compared to the control for global gene expression changes by DAVID analysis; pathways dysregulated in MCF-7 cells after g-C_3N_4 uptake compared to control cells by KEGG pathway analysis; TGFβ pathway is dysregulated by g-C_3N_4; global proteomic changes in cells grown on g-C_3N_4; PDMS scaffolds compared to TCP-grown tenon fibroblast cells; pathways dysregulated in fibroblasts grown on g-C_3N_4-functionalized PDMS; comparison of pathways between microarrays and proteomics-highlighted pathways is common between two studies (XLSX)

■ AUTHOR INFORMATION

Corresponding Authors

Ramaprabhu Sundara − *Department of Physics, Indian Institute of Technology, Madras, Chennai 600036, India;* orcid.org/0000-0002-7960-9470; Email: ramp@iitm.ac.in

Sailaja V. Elchuri − *Department of Nanobiotechnology, Vision Research Foundation, Chennai 600006, India;* orcid.org/0000-0002-9780-2717; Email: sailaja.elchuri@gmail.com

Authors

Chatterjee Amit − *Department of Nanobiotechnology, Vision Research Foundation, Chennai 600006, India*

Gajanan Sathe − *Institute of Bioinformatics, Bangalore 560066, Karnataka, India; Manipal Academy of Higher Education (MAHE), Manipal 576104, Karnataka, India*

Abinaya Shunmugam − *Department of Physics, Indian Institute of Technology, Madras, Chennai 600036, India*

Prasanna Kumar Athyala − *Department of Nanobiotechnology, Vision Research Foundation, Chennai 600006, India*

Vivek Ghose − *Institute of Bioinformatics, Bangalore 560066, Karnataka, India*

Srujana Chitipothu − *Central Research Instrumentation Facility, Core Lab, Vision Research Foundation, Chennai 600006, India*

Narayanan Janakiraman − *Department of Nanobiotechnology, Vision Research Foundation, Chennai 600006, India;* orcid.org/0000-0003-0866-9828

Complete contact information is available at: https://pubs.acs.org/10.1021/acsomega.0c05513

Author Contributions

R.S. and S.V.E. conceived the project. C.A., G.S., A.S., P.K.A., V.G., and N.J. performed experiments; C.A., S.C., G.S., and S.V.E. did data analysis; and C.A. and S.V.E. wrote the manuscript. All authors edited the manuscript.

Notes

The authors declare no competing financial interest.

■ ACKNOWLEDGMENTS

The authors thank SERB, Govt of India (EMR/2015/000607), for the grant to S.V.E., and the Department of Biotechnology, Govt of India (BT/PR26926/NNT/28/1500/2017), for the funding provided to N.J. Authors thank Divya Gopal for help in culturing primary Tenon fibroblast cells.

■ REFERENCES

(1) Allen, M. J.; Tung, V. C.; Kaner, R. B. Honeycomb carbon: a review of graphene. *Chem. Rev.* **2010**, *110*, 132−145.

(2) Mao, H. Y.; Laurent, S.; Chen, W.; Akhavan, O.; Imani, M.; Ashkarran, A. A.; Mahmoudi, M. Graphene: promises, facts, opportunities, and challenges in nanomedicine. *Chem. Rev.* **2013**, *113*, 3407−3424.

(3) Ren, S.; Rong, P.; Yu, Q. Preparations, properties and applications of graphene in functional devices: A concise review. *Ceram. Int.* **2018**, *44*, 11940−11955.

(4) Liu, G.; Jin, W.; Xu, N. Graphene-based membranes. *Chem. Soc. Rev.* **2015**, *44*, 5016−5030.

(5) Chatterjee, N.; Eom, H.-J.; Choi, J. A systems toxicology approach to the surface functionality control of graphene-cell interactions. *Biomaterials* **2014**, *35*, 1109−1127.

(6) Fiorillo, M.; Verre, A. F.; Iliut, M.; Peiris-Pagés, M.; Ozsvari, B.; Gandara, R.; Cappello, A. R.; Sotgia, F.; Vijayaraghavan, A.; Lisanti, M. P. Graphene oxide selectively targets cancer stem cells, across multiple tumor types: implications for non-toxic cancer treatment, via "differentiation-based nano-therapy". *Oncotarget* **2015**, *6*, 3553−3562.

(7) Sun, J.; Zhou, Q.; Hu, X. Integrating multi-omics and regular analyses identifies the molecular responses of zebrafish brains to graphene oxide: Perspectives in environmental criteria. *Ecotoxicol. Environ. Saf.* **2019**, *180*, 269−279.

(8) Orecchioni, M.; Bedognetti, D.; Newman, L.; Fuoco, C.; Spada, F.; Hendrickx, W.; Marincola, F. M.; Sgarrella, F.; Rodrigues, A. F.; Ménard-Moyon, C.; Cesareni, G.; Kostarelos, K.; Bianco, A.; Delogu, L. G. Single-cell mass cytometry and transcriptome profiling reveal the impact of graphene on human immune cells. *Nat. Commun.* **2017**, *8*, No. 1109.

(9) Han, Q.; Chen, N.; Zhang, J.; Qu, L. Graphene/graphitic carbon nitride hybrids for catalysis. *Mater. Horiz.* **2017**, *4*, 832−850.

(10) Pawar, R. C.; Khare, V.; Lee, C. S. Hybrid photocatalysts using graphitic carbon nitride/cadmium sulfide/reduced graphene oxide (g-

C3N4/CdS/RGO) for superior photodegradation of organic pollutants under UV and visible light. *Dalton Trans.* **2014**, *43*, 12514−12527.
(11) Xu, H.; Yan, J.; She, X.; Xu, L.; Xia, J.; Xu, Y.; Song, Y.; Huang, L.; Li, H. Graphene-analogue carbon nitride: novel exfoliation synthesis and its application in photocatalysis and photoelectrochemical selective detection of trace amount of Cu^{2+}. *Nanoscale* **2014**, *6*, 1406−1415.
(12) Brito, W. H.; da Silva-Araújo, J.; Chacham, H. g-C 3 N 4 and Others: Predicting New Nanoporous Carbon Nitride Planar Structures with Distinct Electronic Properties. *J. Phys. Chem. C* **2015**, *119*, 19743−19751.
(13) Zhao, Z.; Sun, Y.; Dong, F. Graphitic carbon nitride based nanocomposites: a review. *Nanoscale* **2015**, *7*, 15−37.
(14) Lin, L.-S.; Cong, Z.-X.; Li, J.; Ke, K.-M.; Guo, S.-S.; Yang, H.-H.; Chen, G.-N. Graphitic-phase C3N4 nanosheets as efficient photosensitizers and pH-responsive drug nanocarriers for cancer imaging and therapy. *J. Mater. Chem. B* **2014**, *2*, 1031−1037.
(15) Li, X.; Zhu, L.; Zhou, Y.; Yin, H.; Ai, S. Enhanced Photoelectrochemical Method for Sensitive Detection of Protein Kinase A Activity Using TiO2/g-C3N4, PAMAM Dendrimer, and Alkaline Phosphatase. *Anal. Chem.* **2017**, *89*, 2369−2376.
(16) Zhang, Y.; Pan, Q.; Chai, G.; Liang, M.; Dong, G.; Zhang, Q.; Qiu, J. Synthesis and luminescence mechanism of multicolor-emitting g-C3N4 nanopowders by low temperature thermal condensation of melamine. *Sci. Rep.* **2013**, *3*, No. 1943.
(17) Zhang, C.; Li, Y.; Zhang, W.; Wang, P.; Wang, C. Metal-free virucidal effects induced by g-C3N4 under visible light irradiation: Statistical analysis and parameter optimization. *Chemosphere* **2018**, *195*, 551−558.
(18) Liu, J.-J.; Chen, Z.-T.; Zhong, Z.; Yan, X.-M.; Kang, L.-T.; Yao, J.-N. Fluorescence-tunable probe for antioxidant capacity assay based on dopamine self-polymerization on graphitic carbon nitride. *Sens. Actuators, B* **2018**, *262*, 570−576.
(19) Wang, Z.; Dong, K.; Liu, Z.; Zhang, Y.; Chen, Z.; Sun, H.; Ren, J.; Qu, X. Activation of biologically relevant levels of reactive oxygen species by Au/g-C3N4 hybrid nanozyme for bacteria killing and wound disinfection. *Biomaterials* **2017**, *113*, 145−157.
(20) Wang, W.; Wu, M.; Liu, G. K. Analysis of Upconversion Fluorescence Dynamics in NaYF 4 Codoped with Er 3+ and Yb 3+. *Spectrosc. Lett.* **2007**, *40*, 259−269.
(21) Cao, Q.; Kumru, B.; Antonietti, M.; Schmidt, B. V. K. J. Graphitic carbon nitride and polymers: a mutual combination for advanced properties. *Mater. Horiz.* **2020**, *7*, 762−786.
(22) Mallinjoud, P.; Villemin, J.-P.; Mortada, H.; Polay Espinoza, M.; Desmet, F.-O.; Samaan, S.; Chautard, E.; Tranchevent, L.-C.; Auboeuf, D. Endothelial, epithelial, and fibroblast cells exhibit specific splicing programs independently of their tissue of origin. *Genome Res.* **2014**, *24*, 511−521.
(23) Selman, M.; Pardo, A. Idiopathic pulmonary fibrosis: an epithelial/fibroblastic cross-talk disorder. *Respir. Res.* **2002**, *3*, 3.
(24) Barua, S.; Mitragotri, S. Challenges associated with Penetration of Nanoparticles across Cell and Tissue Barriers: A Review of Current Status and Future Prospects. *Nano Today* **2014**, *9*, 223−243.
(25) He, H.; Lu, Y.; Qi, J.; Zhu, Q.; Chen, Z.; Wu, W. Adapting liposomes for oral drug delivery. *Acta Pharm. Sin. B* **2019**, *9*, 36−48.
(26) Kristensen, M.; Nielsen, H. M. Cell-penetrating peptides as tools to enhance non-injectable delivery of biopharmaceuticals. *Tissue Barriers* **2016**, *4*, No. e1178369.
(27) Taheri, H.; Unal, M. A.; Sevim, M.; Gurcan, C.; Ekim, O.; Ceylan, A.; Syrgiannis, Z.; Christoforidis, K. C.; Bosi, S.; Ozgenç, O.; Gómez, M. J.; Turktas Erken, M.; Soydal, Ç.; Eroğlu, Z.; Bitirim, C. V.; Cagin, U.; Arı, F.; Ozen, A.; Kuçuk, O.; Delogu, L. G.; Prato, M.; Metin, Ö.; Yilmazer, A. Photocatalytically Active Graphitic Carbon Nitride as an Effective and Safe 2D Material for In Vitro and In Vivo Photodynamic Therapy. *Small* **2020**, *16*, No. 1904619.
(28) Divya, N.; Baro, M.; Ramaprabhu, S. Graphitic Carbon Nitride Hybrid Supported Metal Nanoparticles as a Novel Low-Cost Counter Electrode for Dye-Sensitized Solar Cell. *J. Nanosci. Nanotechnol.* **2016**, *16*, 9583−9590.
(29) Saddala, M. S.; Lennikov, A.; Huang, H. RNA-seq data from C-X-C chemokine receptor type 5 (CXCR5) gene knockout aged mice with retinal degeneration phenotype. *Data Brief* **2020**, *31*, No. 105915.
(30) Saddala, M. S.; Lennikov, A.; Bouras, A.; Huang, H. RNA-Seq reveals differential expression profiles and functional annotation of genes involved in retinal degeneration in Pde6c mutant Danio rerio. *BMC Genomics* **2020**, *21*, 132.
(31) Fina, F.; Callear, S. K.; Carins, G. M.; Irvine, J. T. S. Structural Investigation of Graphitic Carbon Nitride via XRD and Neutron Diffraction. *Chem. Mater.* **2015**, *27*, 2612−2618.
(32) McMillan, P. F.; Lees, V.; Quirico, E.; Montagnac, G.; Sella, A.; Reynard, B.; Simon, P.; Bailey, E.; Deifallah, M.; Corà, F. Graphitic carbon nitride C6N9H3·HCl: Characterisation by UV and near-IR FT Raman spectroscopy. *J. Solid State Chem.* **2009**, *182*, 2670−2677.
(33) Nair, A. A.; Sundara, R.; Anitha, N. Hydrogen storage performance of palladium nanoparticles decorated graphitic carbon nitride. *Int. J. Hydrogen Energy* **2015**, *40*, 3259−3267.
(34) Raghu, S.; Santhosh, P. N.; Ramaprabhu, S. Nanostructured palladium modified graphitic carbon nitride − High performance room temperature hydrogen sensor. *Int. J. Hydrogen Energy* **2016**, *41*, 20779−20786.
(35) Dai, J.; Song, J.; Qiu, Y.; Wei, J.; Hong, Z.; Li, L.; Yang, H. Gold Nanoparticle-Decorated g-C3N4 Nanosheets for Controlled Generation of Reactive Oxygen Species upon 670 nm Laser Illumination. *ACS Appl. Mater. Interfaces* **2019**, *11*, 10589−10596.
(36) Tabish, T. A.; Zhang, S.; Winyard, P. G. Developing the next generation of graphene-based platforms for cancer therapeutics: The potential role of reactive oxygen species. *Redox Biol.* **2018**, *15*, 34−40.
(37) Ou, L.; Lin, S.; Song, B.; Liu, J.; Lai, R.; Shao, L. The mechanisms of graphene-based materials-induced programmed cell death: a review of apoptosis, autophagy, and programmed necrosis. *Int. J. Nanomed.* **2017**, *12*, 6633−6646.
(38) He, N.; Cao, S.; Zhang, L.; Tian, Z.; Chen, H.; Jiang, F. Enhanced photocatalytic disinfection of *Escherichia coli* K-12 by porous g-C3N4 nanosheets: Combined effect of photo-generated and intracellular ROSs. *Chemosphere* **2019**, *235*, 1116−1124.
(39) Heo, N. S.; Shukla, S.; Oh, S. Y.; Bajpai, V. K.; Lee, S. U.; Cho, H.-J.; Kim, S.; Kim, Y.; Kim, H. J.; Lee, S. Y.; Jun, Y.-S.; Oh, M.-H.; Han, Y.-K.; Yoo, S. M.; Huh, Y. S. Shape-controlled assemblies of graphitic carbon nitride polymer for efficient sterilization therapies of water microbial contamination via 2D g-C3N4 under visible light illumination. *Mater. Sci. Eng., C* **2019**, *104*, No. 109846.
(40) Pelin, M.; Fusco, L.; León, V.; Martín, C.; Criado, A.; Sosa, S.; Vázquez, E.; Tubaro, A.; Prato, M. Differential cytotoxic effects of graphene and graphene oxide on skin keratinocytes. *Sci. Rep.* **2017**, *7*, No. 40572.
(41) Turrens, J. F. Mitochondrial formation of reactive oxygen species. *J. Physiol.* **2003**, *552*, 335−344.
(42) Jaworski, S.; Strojny, B.; Sawosz, E.; Wierzbicki, M.; Grodzik, M.; Kutwin, M.; Daniluk, K.; Chwalibog, A. Degradation of Mitochondria and Oxidative Stress as the Main Mechanism of Toxicity of Pristine Graphene on U87 Glioblastoma Cells and Tumors and HS-5 Cells. *Int. J. Mol. Sci.* **2019**, *20*, No. 650.
(43) Fang, Q.; Zhang, Y.; Chen, X.; Li, H.; Cheng, L.; Zhu, W.; Zhang, Z.; Tang, M.; Liu, W.; Wang, H.; Wang, T.; Shen, T.; Chai, R. Three-Dimensional Graphene Enhances Neural Stem Cell Proliferation Through Metabolic Regulation. *Front. Bioeng. Biotechnol.* **2020**, *7*, No. 436.
(44) Kondoh, K.; Nishida, E. Regulation of MAP kinases by MAP kinase phosphatases. *Biochim. Biophys. Acta, Mol. Cell Res.* **2007**, *1773*, 1227−1237.
(45) Heuberger, J.; Birchmeier, W. Interplay of cadherin-mediated cell adhesion and canonical Wnt signaling. *Cold Spring Harbor Perspect. Biol.* **2010**, *2*, No. a002915.

https://doi.org/10.1021/acsomega.0c05513
ACS Omega 2021, 6, 9368−9380

(46) Liu, R.-M.; Desai, L. P. Reciprocal regulation of TGF-β and reactive oxygen species: A perverse cycle for fibrosis. *Redox Biol.* **2015**, *6*, 565−577.
(47) Boutros, R.; Lobjois, V.; Ducommun, B. CDC25 phosphatases in cancer cells: key players? Good targets? *Nat. Rev. Cancer* **2007**, *7*, 495−507.
(48) Ozen, M.; Ittmann, M. Increased expression and activity of CDC25C phosphatase and an alternatively spliced variant in prostate cancer. *Clin. Cancer Res.* **2005**, *11*, 4701−4706.
(49) Safina, I.; Bourdo, S. E.; Algazali, K. M.; Kannarpady, G.; Watanabe, F.; Vang, K. B.; Biris, A. S. Graphene-based 2D constructs for enhanced fibroblast support. *PLoS One* **2020**, *15*, No. e0232670.
(50) Pedraza, E.; Brady, A.-C.; Fraker, C. A.; Stabler, C. L. Synthesis of macroporous poly(dimethylsiloxane) scaffolds for tissue engineering applications. *J. Biomater. Sci., Polym. Ed.* **2013**, *24*, 1041−1056.
(51) Guimont, A.; Beyou, E.; Alcouffe, P.; Martin, G.; Sonntag, P.; Cassagnau, P. Synthesis and characterization of PDMS-grafted graphite oxide sheets. *Polymer* **2013**, *54*, 4830−4837.
(52) Wang, B.; Lee, B.-K.; Kwak, M.-J.; Lee, D.-W. Graphene/polydimethylsiloxane nanocomposite strain sensor. *Rev. Sci. Instrum.* **2013**, *84*, No. 105005.
(53) Sharma, D.; Jia, W.; Long, F.; Pati, S.; Chen, Q.; Qyang, Y.; Lee, B.; Choi, C. K.; Zhao, F. Polydopamine and collagen coated micro-grated polydimethylsiloxane for human mesenchymal stem cell culture. *Bioact. Mater.* **2019**, *4*, 142−150.
(54) Lyra-Leite, D. M.; Andres, A. M.; Petersen, A. P.; Ariyasinghe, N. R.; Cho, N.; Lee, J. A.; Gottlieb, R. A.; McCain, M. L. Mitochondrial function in engineered cardiac tissues is regulated by extracellular matrix elasticity and tissue alignment. *Am. J. Physiol.: Heart Circ. Physiol.* **2017**, *313*, H757−H767.
(55) Lewis, M. P.; Lygoe, K. A.; Nystrom, M. L.; Anderson, W. P.; Speight, P. M.; Marshall, J. F.; Thomas, G. J. Tumour-derived TGF-beta1 modulates myofibroblast differentiation and promotes HGF/SF-dependent invasion of squamous carcinoma cells. *Br. J. Cancer* **2004**, *90*, 822−832.
(56) Ishii, T.; Funato, Y.; Miki, H. Thioredoxin-related protein 32 (TRP32) specifically reduces oxidized phosphatase of regenerating liver (PRL). *J. Biol. Chem.* **2013**, *288*, 7263−7270.
(57) Andersen, K. M.; Madsen, L.; Prag, S.; Johnsen, A. H.; Semple, C. A.; Hendil, K. B.; Hartmann-Petersen, R. Thioredoxin Txnl1/TRP32 is a redox-active cofactor of the 26 S proteasome. *J. Biol. Chem.* **2009**, *284*, 15246−15254.
(58) Sun, Y.; Zheng, Y.; Wang, C.; Liu, Y. Glutathione depletion induces ferroptosis, autophagy, and premature cell senescence in retinal pigment epithelial cells. *Cell Death Dis.* **2018**, *9*, No. 753.
(59) Lv, X.; Li, J.; Zhang, C.; Hu, T.; Li, S.; He, S.; Yan, H.; Tan, Y.; Lei, M.; Wen, M.; Zuo, J. The role of hypoxia-inducible factors in tumor angiogenesis and cell metabolism. *Genes Dis.* **2017**, *4*, 19−24.
(60) Labuschagne, C. F.; Cheung, E. C.; Blagih, J.; Domart, M.-C.; Vousden, K. H. Cell Clustering Promotes a Metabolic Switch that Supports Metastatic Colonization. *Cell Metab.* **2019**, *30*, 720−734.e5.
(61) Sanchez, V. C.; Jachak, A.; Hurt, R. H.; Kane, A. B. Biological interactions of graphene-family nanomaterials: an interdisciplinary review. *Chem. Res. Toxicol.* **2012**, *25*, 15−34.
(62) Lian, N.; Wang, W.; Li, L.; Elefteriou, F.; Yang, X. Vimentin inhibits ATF4-mediated osteocalcin transcription and osteoblast differentiation. *J. Biol. Chem.* **2009**, *284*, 30518−30525.

https://doi.org/10.1021/acsomega.0c05513
ACS Omega 2021, 6, 9368−9380